Geophys. J. Int. (2000) **143,** 328–334

A semi-numerical method for elastic wave scattering calculations

Ajit Mal[1] and Zensheu Chang[2]

[1] *Mechanical and Aerospace Engineering Department, University of California, Los Angeles,* CA 90095-1597, *USA. E-mail: ajit@ucla.edu*
[2] *Jet Propulsion Laboratory, Mail Stop* 67-119, *Pasadena,* CA 91109, *USA*

Accepted 2000 May 31. Received 2000 April 3; in original form 1999 November 30

SUMMARY

This paper is concerned with the calculation of elastic wavefields in strongly heterogeneous media containing scatterers of arbitrary shape and size. A hybrid method is described in which the elastodynamic field within a finite region enclosing the scatterers is modelled by finite elements while the field away from this region is represented by means of a suitable set of wave functions. Application of a variational principle and the continuity conditions at the interface between the two regions lead to a system of linear equations that is solved by standard techniques. The hybrid method extends the applicability of the finite element method to wave propagation problems in unbounded media by rigorously modelling the radiation field. The method is used to calculate the elastodynamic field in a plate of finite thickness and infinite lateral dimensions containing geometric discontinuities.

Key words: finite elements, Lamb waves, scattering.

INTRODUCTION

The calculation of elastic wavefields in heterogeneous media is of great interest in a variety of applications, including strong ground motion simulation for earthquake-resistant design, seismic tomography to determine the Earth's internal constitution, non-destructive evaluation to detect and characterize flaws in critical structural components, etc. There is a vast amount of literature on the interaction of elastic waves with single as well as multiple inhomogeneities, and no attempt will be made to describe it here. It should be noted that asymptotic theories valid at low or high frequencies have been the mainstay of early work on the subject and have provided valuable physical insight into the qualitative features of the interaction phenomena. However, the asymptotic techniques lose their accuracy in the intermediate frequency range where the interaction effects are most pronounced, more interesting and more useful for practical applications. Analytical techniques that can be applied in the entire frequency range are limited to relatively simple geometry of the scatterers, for example cylinders and spheres (see, for example, Knopoff 1959a,b; Gilbert & Knopoff 1959, 1961; Mal & Bose 1974; Yang & Mal 1994). Modern applications require the availability of calculation models that can simulate wave interaction phenomena in media containing scatterers of arbitrary shape and size at all frequencies.

Although the finite element method (FEM) provides a convenient and powerful means for representing the inhomogeneous region, its conventional implementation encounters difficulty in modelling the radiated field external to the discretized region. An alternative procedure is to employ a time domain formulation in a finite region if the interest is limited to small time windows. However, the observed dissipative properties of most materials indicate that it is difficult, if not impossible, to express their constitutive equations in the time domain. Thus, for calculations that are valid for large time windows and where the dissipative properties of the materials are significant, the frequency domain formulation is preferable. Other potentially useful semi-numerical methods include the boundary integral equation method (see, for example, Dravinski 1984) and the volume integral equation method (Mal & Knopoff 1967; Lee & Mal 1995).

In what follows, a recently developed hybrid technique incorporating the widely used finite element method (FEM) near the inhomogeneity and analytical representation of the wave functions in the far field is described. The hybrid technique can extend the range of application of FEM to unbounded media without the need to discretize large regions (see, for example, Goetschel *et al.* 1982). In this paper, the hybrid method is applied to the problem of a plate containing geometrical discontinuities as an illustrative example.

The interaction of Lamb waves with a free edge of a plate was first studied by Torvik (1967), who used a variational technique to derive the modal coefficients. In addition, the partition of energy among different modes above the first cut-off frequency was studied. Using the projection method, Gregory & Gladwell

(1983) studied the free-edge reflection problem and extended the frequency range investigated by Torvik (1967). In both cases, the first symmetric mode Lamb wave was used as the incident wave. The anti-symmetric case was not considered in either study. The conventional FEM was applied to plates with defects by Alleyn & Cawley (1992), and a hybrid method was used by Datta, Al-Nassar & Shah (1991) to calculate the waves scattered by a crack within a plate. In this paper, the 2-D (in-plane) problem of Lamb wave propagation in a plate of finite thickness and infinite lateral dimensions containing defects on one of its surfaces is considered. A 3-D problem of the plate has been considered in Chang & Mal (1999).

THE HYBRID TECHNIQUE

The geometry of the general problem is depicted in Fig. 1, where the material (henceforth referred to as the *inclusion*) bounded by the surface S has properties significantly different from those outside S (the *matrix*). The inclusion itself can be heterogeneous, anisotropic and viscoelastic. The matrix is assumed to be homogeneous, isotropic and viscoelastic for the sake of simplicity. The waves are assumed to be generated by sources external to the inclusion.

Let $\mathbf{u}(\mathbf{x}, \omega)$ denote the Fourier time transform of the displacement vector at a point x within the solid. Then $\mathbf{u}(\mathbf{x}, \omega)$ is, in general, a complex, frequency-dependent function and is the solution of a time-harmonic boundary value problem in which all field variables have the time dependence $\exp(-i\omega t)$. The time domain solution can be easily obtained through inversion using FFT or other suitable algorithms. In what follows we consider time-harmonic problems only, and suppress the common time dependence as well as the frequency dependence in all field variables. The Cartesian components of the stress tensor, τ, are related to the components of the displacement through the appropriate constitutive equation. The displacement vector $\mathbf{u}$ satisfies Navier's equations and is continuous everywhere except at the source. The stress vector is continuous across all surface elements including those where a sharp transition in material properties may occur. In addition, for an unbounded matrix, the field must represent outgoing waves or satisfy a radiation condition at infinity.

In order to illustrate the frequency domain hybrid method for unbounded media, assume that a plane time-harmonic wave is incident on an irregularly shaped inclusion perfectly bonded to the matrix at the interface S, and introduce a surface B containing the inclusion as the FEM mesh boundary. The region inside B is discretized and analysed by the finite element method, and the behaviour of the region outside B is represented by a set of *global wave functions*. The continuity of the displacement and traction on the mesh boundary must be satisfied through proper choice of the amplitudes of the global functions.

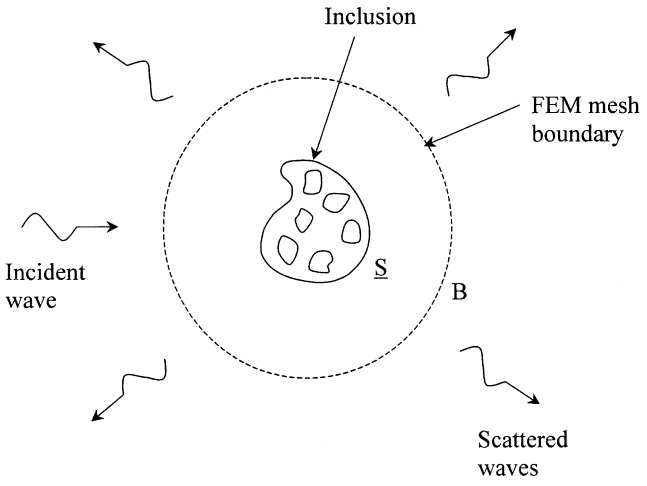

Figure 1. The hybrid model of the general wave scattering problem.

The global functions are the displacements that satisfy the governing equation and the boundary conditions of the same problem in the absence of the inclusion, and will be denoted by g_n ($n=1, 2, \ldots$). Assume that the displacements associated with the incident wave $\mathbf{u}^{\mathbf{I}}$ and the scattered wave $\mathbf{u}^{\mathbf{S}}$ outside B can be expressed in the forms

$$\mathbf{u}^{\mathbf{I}} = \sum_{n=1}^{p} a_n \mathbf{g}_n , \tag{1a}$$

$$\mathbf{u}^{\mathbf{S}} = \sum_{n=1}^{q} b_n \mathbf{g}_n , \tag{1b}$$

where p, q are integers to be selected based on the required accuracy, the constants a_n are known, and the constants b_n are to be determined from the continuity conditions on the mesh boundary. The finite element formulation is based on the minimization of the functional

$$\Pi = \int_V \left[\rho\omega^2 u_i u_i^* - \frac{\tau_{ij} u_{i,j}^*}{2} + f_i u_i^* \right] dV + \int_B \tau_{ij} u_i^* n_j \, dS , \tag{2}$$

where ρ is the density of the material, an asterisk implies complex conjugation, $\mathbf{f}$ is the body force, and $\mathbf{n}$ is the unit vector normal to B. In the conventional finite element technique, either the displacement u_i or the stress vector $\tau_{ij} n_j$ is prescribed on B, but the boundary conditions for the present problem are of a different type, as will be seen below.

Using the conventional finite element discretization of the field inside the mesh boundary, B, and applying the variational principle based on the minimization of (2), we obtain a system of linear equations relating the nodal displacements to the nodal forces. For convenience, we divide both the displacement and the force vectors into two parts: one part is associated with the nodes interior to the mesh boundary; and the other part is for the boundary nodes. The linear equations can be expressed in block matrix notation as follows:

$$\begin{bmatrix} D_{\mathrm{ii}} & D_{\mathrm{ib}} \\ D_{\mathrm{bi}} & D_{\mathrm{bb}} \end{bmatrix} \begin{Bmatrix} U_{\mathrm{i}} \\ U_{\mathrm{b}} \end{Bmatrix} = \begin{Bmatrix} F_{\mathrm{i}} \\ F_{\mathrm{b}} \end{Bmatrix}, \tag{3}$$

where the subscript b refers to the boundary, and the subscript i refers to the interior, $\{U\}$ is the column vector of the nodal displacements, and $\{F\}$ is the column vector of the nodal forces. The matrix $[D_{\mathrm{ii}}]$ relates the interior nodal displacements to the interior nodal forces, $[D_{\mathrm{bb}}]$ relates those on the boundary, $[D_{\mathrm{ib}}]$ and $[D_{\mathrm{bi}}]$ are the coupling matrices between the interior and boundary nodes.

For the time being, we only consider the field variables at the nodes on the mesh boundary. From (1a), we can derive the values of both the displacement and the force vectors corresponding to the incident wave at the nodes on the mesh boundary, by substituting the coordinates of the boundary nodes into the

global functions. Thus

$$\{U_b^I\} = \sum_{n=1}^{p} a_n \{G_n\}, \tag{4}$$

$$\{F_b^I\} = \sum_{n=1}^{p} a_n \{F_n\}, \tag{5}$$

where $\{G_n\}$ is the vector composed of the values of the global functions g_n on the mesh boundary, and $\{F_n\}$ is the associated force vector.

Using each displacement vector $\{G_n\}$ in (4) as the boundary condition on B, and by the conventional finite element approach, we obtain the corresponding boundary forces:

$$\{F_b^I\}_{FEM} = \sum_{n=1}^{p} a_n \{V_{nb}\}, \tag{6}$$

where the vector $\{V_{nb}\}$ is the result of using the displacement vector $\{G_n\}$ in (4) as the boundary condition. The subscript 'FEM' implies that the vector is derived from the interior finite element.

Similarly, we can derive the displacement and force vectors associated with the scattered field:

$$\{U_b^S\} = \sum_{n=1}^{q} b_n \{G_n\}, \tag{7}$$

$$\{F_b^S\} = \sum_{n=1}^{q} b_n \{F_n\}, \tag{8}$$

$$\{F_b^S\}_{FEM} = \sum_{n=1}^{q} b_n \{V_{nb}\}. \tag{9}$$

Clearly, the displacement continuity across the mesh boundary is automatically satisfied, since we have used the displacement vectors derived from the global functions as the boundary conditions for the discretized region. Thus the only continuity condition that remains to be satisfied is the nodal force condition. There are two sets of force vectors on the mesh boundary—one from the global functions, the other from the finite element model—and each set contains both the incident and the scattered parts. The next step is to find a set of unknown amplitudes b_n that minimizes the difference between the two force vectors. Equating the boundary nodal force vectors from the global functions to those from the finite element method, we obtain

$$\begin{aligned}\{F_b^I\} + \{F_b^S\} &= \sum_{n=1}^{p} a_n \{F_n\} + \sum_{n=1}^{q} b_n \{F_n\} \\ &= \{F_b^I\}_{FEM} + \{F_b^S\}_{FEM} \\ &= \sum_{n=1}^{p} a_n \{V_{nb}\} + \sum_{n=1}^{q} b_n \{V_{nb}\}. \end{aligned} \tag{10}$$

This leads to a system of linear equations for b_n of the form

$$\sum_{n=1}^{q} b_n (\{F_n\} - \{V_{nb}\}) = \sum_{n=1}^{p} a_n (\{V_{nb}\} - \{F_n\}), \tag{11}$$

which can be expressed in matrix form as

$$[A]_{m\times q}\{b\}_{q\times 1} = \{c\}_{m\times 1}. \tag{12}$$

In (12) the elements of the matrix $[A]$ and the vectors $\{b\}$ and $\{c\}$ are all complex, m is the total number of nodes on the mesh boundary, and q is the total number of global functions used to represent the scattered field. Since m is usually greater than q, the unknowns b_n can be solved by applying the least-squares method, which minimizes the difference between the left- and right-hand sides of (12). This is equivalent to minimizing the difference between the displacement fields just inside and just outside the mesh boundary. This minimization leads to the standard linear system

$$([A^*]^T_{q\times m}[A]_{m\times q})\{b\}_{q\times 1} = [A^*]^T_{q\times m}\{c\}_{m\times 1}, \tag{13}$$

where the asterisk indicates the complex conjugate, and the superscript T indicates a transpose. Once the global functions are known, the system of equations (13) can be solved by means of standard techniques. The hybrid formulation has been applied to the solution of problems of special interest in the inspection of ageing aircraft structures involving guided wave propagation in a plate with geometric discontinuities. Representative results are presented below.

The global functions for a plate

For a plate, Lamb waves are used as the global functions. In the 2-D case, the motion due to Lamb waves can be decomposed into *symmetric* and *anti-symmetric* modes. The displacement components U along the x-axis and V along the y-axis, associated with the two modes in the plate occupying the region $-\infty < x < \infty$, $-H < y < H$, (Fig. 2a) can be expressed in the forms given below (see, for example, Mal & Singh 1991).

Symmetric mode

$$\begin{aligned} U(x, y) &= [ik\cosh(\eta_1 y) - \eta_2 C\cosh(\eta_2 y)]\, e^{ikx}, \\ V(x, y) &= [\eta_1 \sinh(\eta_1 y) + ikC\sinh(\eta_2 y)]\, e^{ikx}, \end{aligned} \tag{14}$$

where

$$C = -\frac{(2k^2 - k_2^2)\cosh(\eta_1 H)}{2ik\eta_2 \cosh(\eta_2 H)}, \tag{15}$$

$$\begin{aligned} \eta_j &= \sqrt{k^2 - k_j^2}, \quad |k| > k_j \\ &= i\sqrt{k_j^2 - k^2}, \quad |k| < k_j, \end{aligned} \tag{16}$$

$$k_j = \omega/c_j, \quad j = 1, 2,$$

c_1 and c_2 are the P- and S-wave speeds in the solid. The associated dispersion equation is

$$\frac{\tanh(\eta_1 H)}{\tanh(\eta_2 H)} = \frac{(2k^2 - k_2^2)^2}{4k^2\eta_1\eta_2}. \tag{17}$$

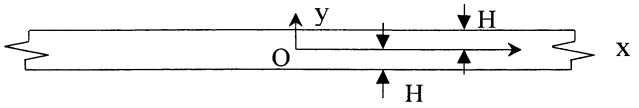

Figure 2. The geometry of a plate without defects.

Anti-symmetric mode

$$U(x, y) = [ik \sinh(\eta_1 y) - \eta_2 D \sinh(\eta_2 y)]\, e^{ikx},$$
$$V(x, y) = [\eta_1 \sinh(\eta_1 y) - ikD \sinh(\eta_2 y)]\, e^{ikx}, \quad (18)$$

where

$$D = -\frac{(2k^2 - k_2^2)\sinh(\eta_1 H)}{2ik\eta_2 \sinh(\eta_2 H)}. \quad (19)$$

The associated dispersion equation is

$$\frac{\tanh(\eta_2 H)}{\tanh(\eta_1 H)} = \frac{(2k^2 - k_2^2)^2}{4k^2\eta_1\eta_2}. \quad (20)$$

The global function $\mathbf{g}_n$ is the vector $\{U, V\}$ calculated at $k = k_n$, where k_n is the nth root of the dispersion equation (17) or (20). The expressions for the global functions given in (14) and (18) represent, respectively, symmetric and anti-symmetric Lamb waves propagating to the right. The global function associated with the Lamb waves propagating to the left is simply $\mathbf{g}_n^*$, the complex conjugate of $\mathbf{g}_n$. It should be noted that the roots of (17) and (20) can be real or complex. At a given frequency, these equations have a finite number of real roots and an infinite number of pure imaginary or complex roots. The real roots are associated with the propagating modes; their amplitude remains constant at points away from the source. The complex roots are associated with non-propagating modes; their amplitude decays exponentially with distance from the source. In the present problem, the geometrical boundaries of the defects act as virtual sources for both propagating and non-propagating waves. In the vicinity of the defects, the contributions to the wavefield from the two types of waves are comparable, but the relative strength of the non-propagating modes decreases away from the defects. It has been shown by Vasudevan & Mal (1985) that the effect of the non-propagating modes can be ignored at points about twice the plate thickness away from the source. Thus if the mesh boundary is located at least twice the plate thickness away from the defects, the non-propagating modes can be ignored outside the mesh boundary and only the propagating modes can be used as the global functions. The material properties of the plate used in the numerical calculation are $2H = 1.6$ mm, $c_1 = 6.4$ km s^{-1}, $c_2 = 3.1$ km s^{-1}, density $\rho = 2.8$ g cm^{-3}. The dispersion curves for symmetric and anti-symmetric Lamb waves are shown in Fig. 3. It should be noted that at a fixed frequency there are a small number of propagating modes and an additional mode is added at each cut-off frequency.

LAMB WAVES IN A SEMI-INFINITE PLATE WITH DEFECTS

In order to illustrate the application of the hybrid technique to wave scattering problems, the propagation of Lamb waves in a semi-infinite plate with a surface defect under plane strain conditions is considered next. The plate is divided into two parts by the mesh boundary as shown in Fig. 4. The region between the mesh boundary and the free edge of the plate is analysed by the finite element method, while the behaviour of waves in the semi-infinite plate on the left side of the mesh boundary is represented by the Lamb wave modal expansion. Application of the continuity conditions across the mesh boundary leads to a system of overdetermined, complex, linear

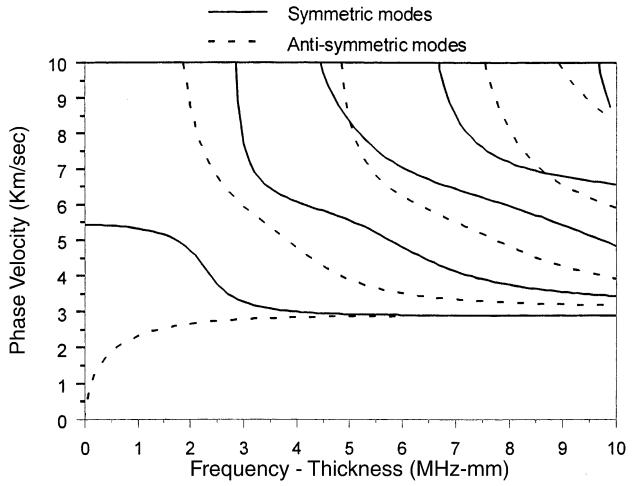

Figure 3. Lamb wave dispersion curves.

equations, which is solved by the least-squares method. The mesh boundary is located at a distance of 10 times the plate thickness away from the free edge. The fundamental symmetric (S_0) and anti-symmetric (A_0) modes are used as incident waves.

We first present some of our calculated results in the absence of the defect. The fundamental symmetric (S_0) and anti-symmetric (A_0) modes are used as incident waves. Clearly, an incident symmetric mode is reflected as symmetric modes only, and an anti-symmetric mode is reflected as anti-symmetric modes. Moreover, in the frequency range below the first cut-off frequency (approximately 0.97 MHz for the anti-symmetric mode and 1.48 MHz for the symmetric mode), only the corresponding fundamental mode is reflected, and the amplitude is the same as that of the incident wave. However, at higher frequencies, higher modes are induced in addition to the fundamental mode, and the global functions must include an adequate number of these modes. The number of modes to be included depends on the frequency range of interest. As an example, if the incident wave is the S_0 mode, then $p = 1$, and q is the number of possible modes at the maximum frequency of interest.

The real and imaginary parts of the vertical displacement on the top surface calculated by means of the hybrid method for both the symmetric and anti-symmetric cases at low frequencies are shown in Fig. 5. At these frequencies, the displacement is pure imaginary for the symmetric case, as shown in the figure, while for the anti-symmetric case the real and imaginary parts of the displacement are equal. Both of these cases represent standing waves within the plate. It can also be seen that, for the anti-symmetric case, the displacement is larger at the free edge and becomes sinusoidal at distances away from the free edge. This is because the non-propagating modes are also induced when the incident wave strikes the free edge; their influence decreases away from the edge. In contrast, the displacement at the free edge is almost non-existent in the symmetric case. This is because the symmetric non-propagating modes have very little effect on the reflected field, and the incident and reflected propagating modes cancel each other at the free edge.

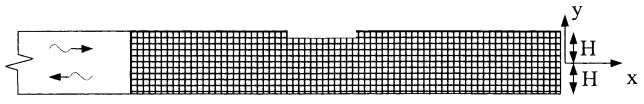

Figure 4. The hybrid model of a semi-infinite plate with a surface defect.

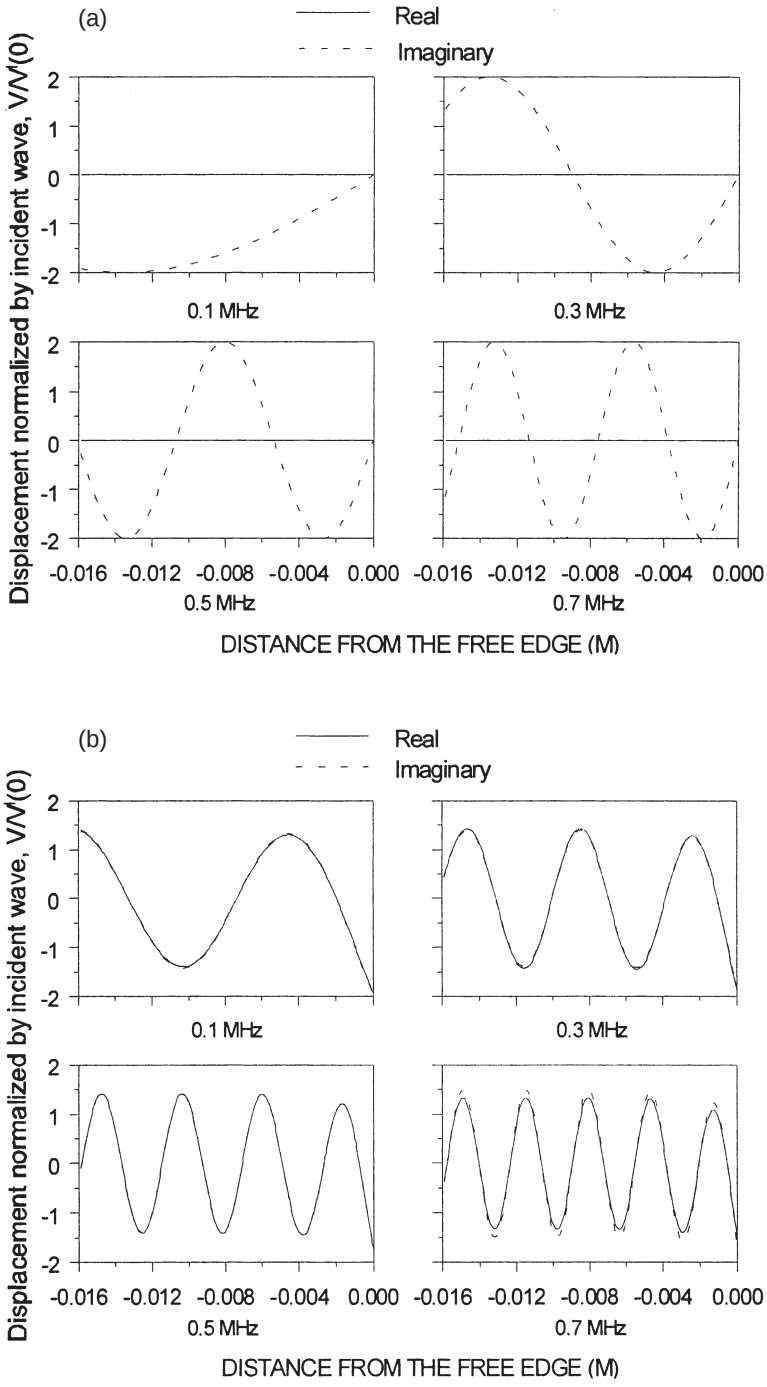

Figure 5. Real and imaginary parts of the vertical surface displacement calculated from the global–local finite element method. Displacements are normalized to the incident amplitude. (a) Symmetric case. (b) Anti-symmetric case.

The real and imaginary parts of the reflected waves are plotted in Fig. 6. It can be seen that, at frequencies below the first cut-off, the symmetric reflected waves suffer a phase reversal as compared to the incident wave. For the anti-symmetric case, the phase shift is 90°, but it changes rapidly near the first cut-off frequency of 0.97 MHz. A similar rapid change in phase occurs in the symmetric case at 1.48 MHz, the corresponding cut-off frequency. These effects were also observed by Torvik (1967) in the symmetric case. An interesting feature of the solution is the behaviour of the waves at the cut-off frequencies. The vertical displacement at the symmetric resonant frequency of 1.48 MHz is shown in Fig. 7. It can be seen that the displacement at the free edge is about seven times higher than that away from the free edge.

A semi-infinite plate with surface defects is considered next. Defects of various widths and depths are introduced at the top surface of the plate. The fundamental symmetric mode is used as the incident wave; the waveform is assumed to consist of a train of cosine waves modulated by a Gaussian envelope. The reflected waveforms calculated from the hybrid method are shown in Figs 8 and 9. It can be seen that the depth of the defect has a stronger effect on the reflection than the width.

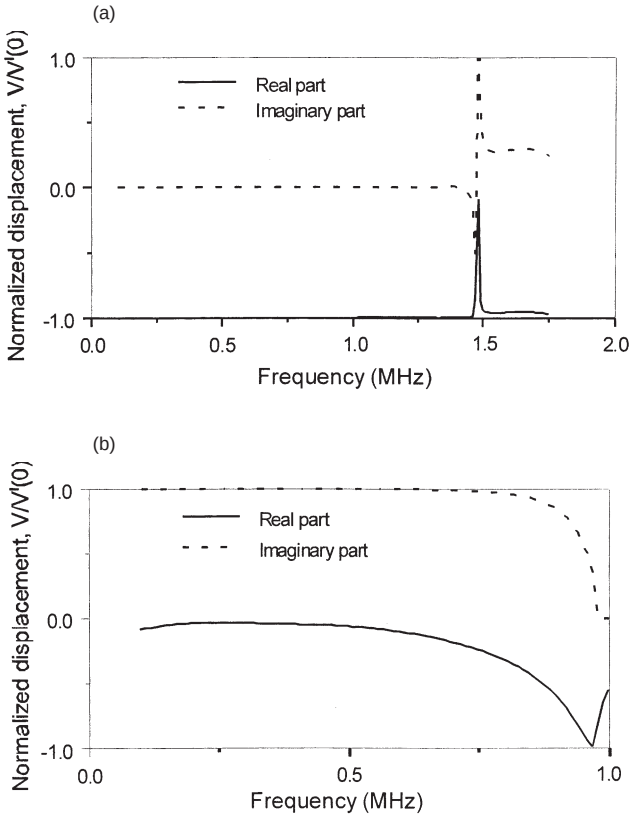

Figure 6. Real and imaginary parts of the normalized vertical surface amplitude of the reflected waves showing the influence of cut-off frequency. (a) Symmetric case: the first cut-off frequency is about 1.48 MHz. (b) Anti-symmetric case: the first cut-off frequency is about 0.97 MHz.

All reflections have one feature in common: the reflected signal can be roughly divided into three parts. The first part is the reflection from the defect. The second part is the wave transmitted across the defect, then reflected by the free edge and propagating across the defect again to the transducer. The last part is the wave reflected by the free edge twice and then propagating across the defect. Theoretically, an infinite number of wave trains are reflected between the defect and the free

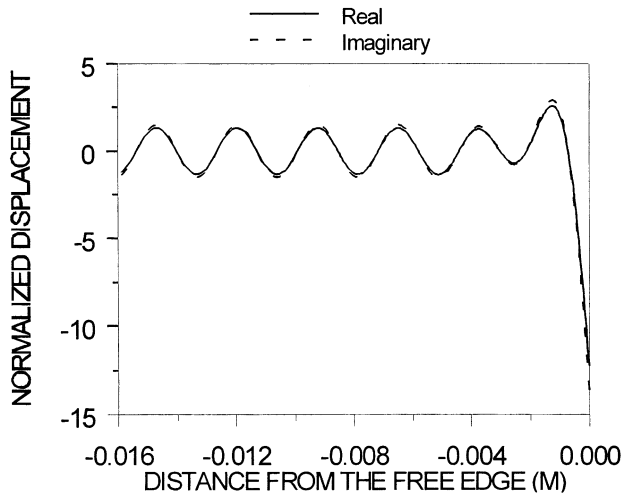

Figure 7. Top surface displacement at the cut-off frequency, 1.48 MHz, for the symmetric case.

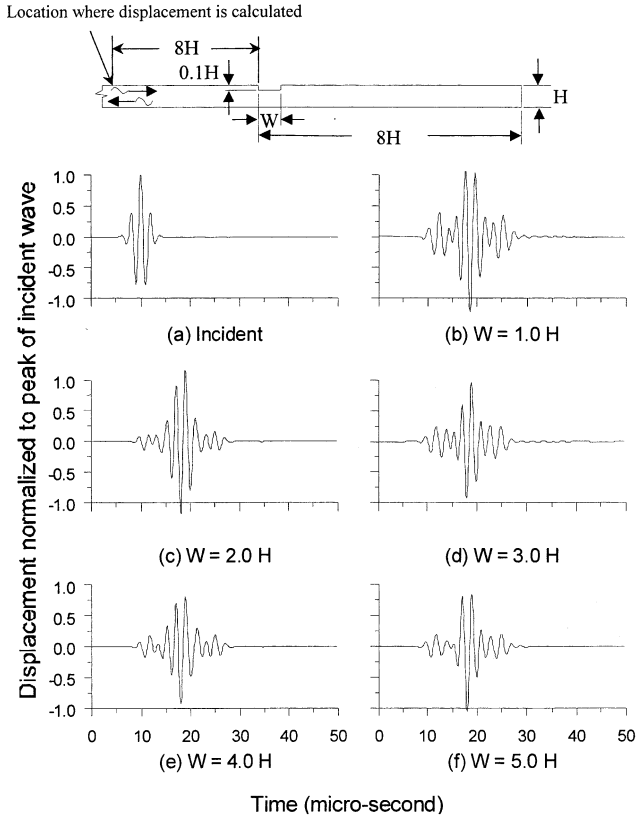

Figure 8. Vertical displacement at the location shown due to the incident and reflected waves from a wide surface defect. ($H = 1.6$ mm).

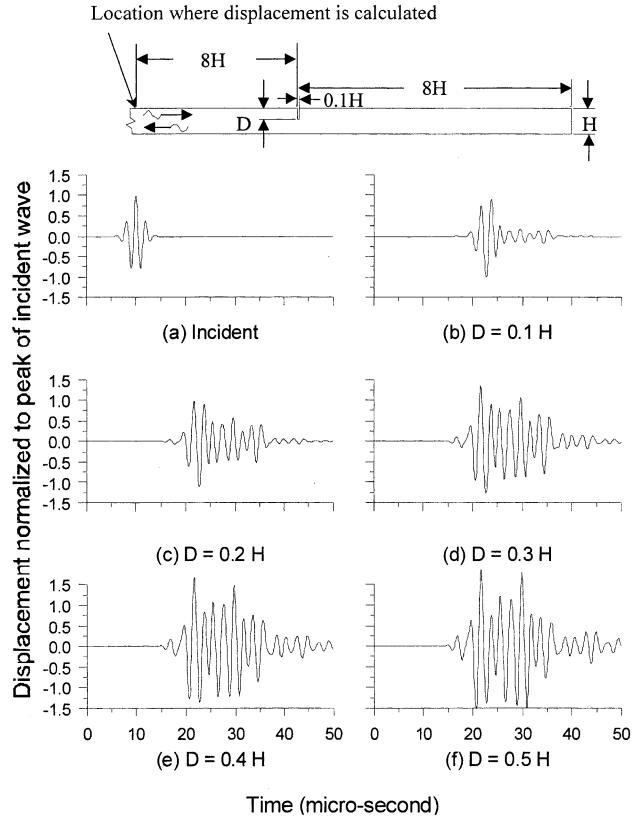

Figure 9. As Fig. 8, but for a narrow surface defect.

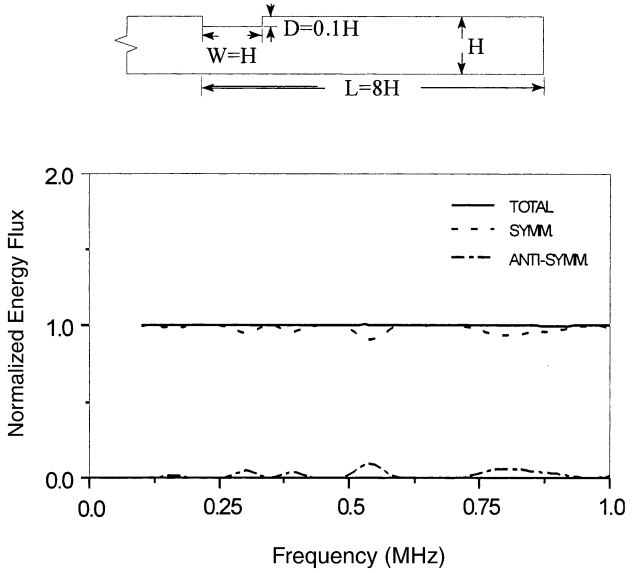

Figure 10. Partition of energy in various reflected modes for a wide surface defect.

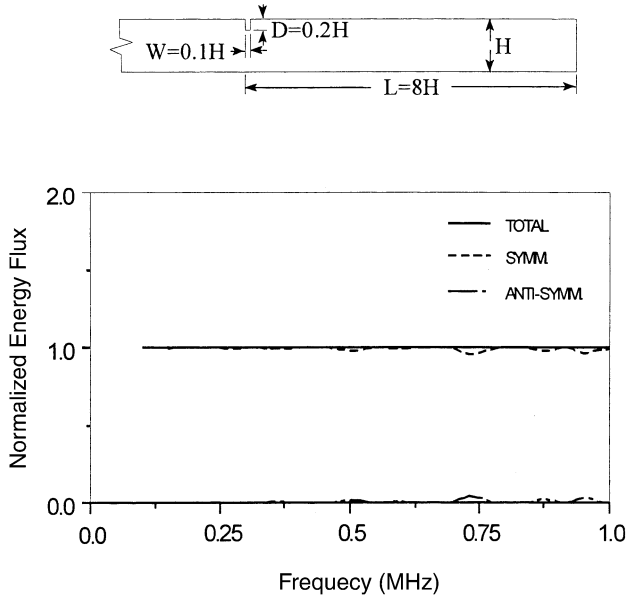

Figure 11. Partition of energy in various reflected modes for a narrow surface defect.

edge. All except the three signals described above are too small to be identified in the received signal, since only a very small portion of the energy is reflected each time the wave comes across the defect.

It should be noted that in both Figs 8 and 9 the reflected waves have larger amplitude than the incident waves. The increase in amplitude is caused by the interference between the reflected waves from the right edge of the plate and the defect. In order to verify that the amplitude increase in the reflected field does not violate the energy principle, the energy flux through a vertical surface S_1 (x = constant) associated with the waves is calculated from the formula

$$E_f = -\frac{\omega}{2}\int_{S_1} \tau_{i1} u_i^* \, dS . \tag{21}$$

The energy flux for each wave normalized to that in the incident wave is shown in Figs 10 and 11. It can be seen that the total energy flux is unity in both cases, implying that energy is conserved. The results also show that, when the symmetric incident waves are reflected from the free edges of a plate with defects, most of the energy remains in the symmetric mode; only a small portion is converted into the anti-symmetric mode.

CONCLUDING REMARKS

The hybrid technique described in this paper is a rigorous extension of the conventional finite element method to wave propagation problems in extended media. It takes full advantage of the capability of the conventional finite element method in modelling complex media, and uses the classical analytical solutions of canonical problems to remove the difficulty associated with the FEM in modelling the radiated field. In addition to the plate problems discussed here, the method can be applied to wave propagation problems in laterally heterogeneous layered earth models.

REFERENCES

Alleyne, D.N. & Cawley, P., 1992. The interaction of Lamb waves with defects, *IEEE Trans. on Ultrasonics, Ferroelectrics, Frequency Control.,* **39,** 381–397.

Chang, Z. & Mal, A., 1999. Scattering of Lamb waves from a rivet hole with edge cracks, *Mech. Mat.,* **31,** 197–204.

Datta, S.K., Al-Nassar, Y. & Shah, A.H., 1991. Lamb wave scattering by a surface-breaking crack in a plate, in *Review of Progress in Quantitative NDE,* Vol. 10A, pp. 79–104, eds Thompson, D.O. & Chimenti, D.E., Plenum, New York.

Dravinski, M., 1984. Evaluation of strong ground motion using boundary integral equation approach, in *Earthquake Source Modeling, Ground Motion and Structural Response*, pp. 61–80, ed. Datta, S.K., ASME-AMD, Vol. 60.

Gilbert, J.F. & Knopoff, L., 1959. Scattering of impulsive elastic waves by a rigid cylinder, *J. acoust. Soc. Am.,* **31,** 1169–1175.

Gilbert, J.F. & Knopoff, L., 1961. Diffraction of elastic waves by the core of the earth, *Bull. seism. Soc. Am.,* **51,** 35–39.

Goetschel, D.B., Dong, S.B. & Muki, R., 1982. A global local finite element analysis of axisymmetric scattering of elastic waves, *J. appl. Mech.,* **49,** 816–820.

Gregory, R.D. & Gladwell, I., 1983. The reflection of a symmetric Rayleigh–Lamb wave at the fixed or free edge of a plate, *J. Elasticity,* **13,** 185–206.

Knopoff, L., 1959a. Scattering of compression waves by spherical obstacles, *Geophysics,* **24,** 30–39.

Knopoff, L., 1959b. Scattering of shear waves by spherical obstacles, *Geophysics,* **24,** 209–219.

Lee, J.-K. & Mal, A.K., 1995. A volume integral equation technique for multiple scattering problems in elastodynamics, *Appl. Math. Comput.,* **67,** 135–159.

Mal, A.K. & Bose, S.K., 1974. Dynamic elastic moduli of a suspension of imperfectly bonded spheres, *Proc. Camb. Phil. Soc.,* **76,** 587–600.

Mal, A.K. & Knopoff, L., 1967. Elastic wave velocities in two component systems, *J. Inst. math Applic.,* **3,** 376–387.

Mal, A.K. & Singh, S.J., 1991. *Deformation of Elastic Solids,* Prentice Hall, Englewood Cliffs, NJ.

Torvik, P.J., 1967. Reflection of wave trains in semi-infinite plates, *J. acoust. Soc. Am.,* **41,** 346–353.

Vasudevan, N. & Mal, A.K., 1985. Response of an elastic plate to localized transient sources, *J. appl. Mech.,* **107,** 356–362.

Yang, R.-B. & Mal, A.K., 1994. Multiple scattering of elastic waves in a fiber-reinforced composite, *J. Mech. Phys. Sol.,* **42,** 1945–1968.